Fermi-Surface Topology and Helical Antiferromagnetism in Heavy Lanthanide Metals

K. M. Döbrich,[1,2] A. Bostwick,[3] J. L. McChesney,[3] K. Rossnagel,[3,*] E. Rotenberg,[3] and G. Kaindl[1]

[1]*Institut für Experimentalphysik, Freie Universität Berlin, Arnimallee 14, 14195 Berlin-Dahlem, Germany*

[2]*Max-Born-Institut, Max-Born-Straße 2A, 12489 Berlin, Germany*

[3]*Advanced Light Source, Lawrence Berkeley National Laboratory, Berkeley, California 94720, USA*

(Received 16 March 2010; published 15 June 2010)

Detailed angle-resolved photoemission studies of Tb and Dy metal in the paramagnetic phase provide direct experimental proof of the presence of nesting features in the Fermi surfaces (FS) of these heavy lanthanide (Ln) metals. The observations clearly support the hypothesis that nesting of the FS in the paramagnetic phase is responsible for the development of helical antiferromagnetic ordering in heavy Ln metals. They also show that magnetic exchange splitting of the electronic states is responsible for the disappearance of FS nesting in the ferromagnetic phases.

DOI: 10.1103/PhysRevLett.104.246401 PACS numbers: 71.18.+y, 71.20.Eh, 75.50.Cc, 79.60.−i

A detailed knowledge of the topology of the Fermi surface (FS) is the key to understanding the variety of magnetic ordering phenomena in heavy lanthanide (Ln) metals (Gd–Tm), such as the development of helical antiferromagnetic (AFM), conical ferrimagnetic, and ferromagnetic (FM) phases [1]. The origin of these magnetic structures lies in the localized electrons of the partially filled $4f$ shell that can couple between neighboring atoms only in an indirect way via conduction electrons [Ruderman-Kittel-Kasuya-Yoshida (RKKY) interaction]. Most of the heavy Ln metals have the same conduction-electron configuration $(5d6s)^3$, resulting in rather similar chemical properties. Minor differences in the lattice constants of a few percent, caused by a reduction of the size of the Wigner-Seitz radius due to Ln contraction, and a simultaneous reduction of the c/a ratio, however, lead to decisive differences in the topology of the FS within the Ln series [2].

The helical AFM phase, observed in some of the heavy Ln metals, is believed to be the manifestation of a spin-density wave (SDW), which originates from the topology of the FS. The so-called nesting of the FS in the paramagnetic (PM) phase, due to approximately parallel sheets, separated by a nesting vector $\mathbf{q_0}$ in $\mathbf{k}$ space [see schematics in Fig. 1(a)], leads to singularities in the magnetic susceptibility $\chi(\mathbf{q})$ at $\mathbf{q} = \mathbf{q_0}$ [3,4], where $\mathbf{q_0}$ is parallel to the k_z axis. As a consequence, the total energy of the spin system $E(\mathbf{q})$ exhibits a minimum at $\mathbf{q_0}$, corresponding to a SDW with helical arrangement of the magnetic moments with a periodicity in real space of $2\pi/|\mathbf{q_0}|$. The connection between FS nesting and the development of a helical SDW in a Ln metal is commonly referred to as the ''nesting hypothesis.'' For a pure Ln metal, FS nesting has not been observed in a direct experiment to date, and there is also no study of its behavior at a magnetic phase transition.

Rather indirect support for the nesting hypothesis had been provided from electrical resistivity and magnetic susceptibility studies of Tb metal under hydrostatic pressure or uniaxial stress [5]. For nonmagnetic Y metal and Gd-Y alloys in the PM phase, FS nesting had been seen in positron-annihilation studies [6–8]; for pure Gd metal in the PM phase, however, no FS nesting was found. These latter results were confirmed in Ref. [9] by angle-resolved photoelectron spectroscopy (ARPES), where also drastic changes of the FS upon FM ordering were seen. Theory predicts FS nesting in the PM phases of Tb, Dy, Ho, Er, and Tm metal around the L point of the hexagonal Brillouin zone (BZ), but absence of nesting for Gd [2,10,11]. Up to now, experimental FS studies for Tb metal are available only for the FM phase where no FS nesting was observed, in agreement with theory [12,13]. This is in accordance with Liu [4], who argued on the basis of a theoretical model that the magnetic exchange splitting of valence states, ΔE_{ex}, lifts the degeneracy of majority and minority FS sheets, causing FS nesting to disappear. This mechanism could then be the driving force behind the AFM-to-FM phase transitions in these magnetic systems. So far, no experimental proof of this hypothesis has been provided.

In this Letter, we present the results of extensive ARPES studies of Tb and Dy metal that prove the presence of FS nesting in the PM phases of these two Ln metals with helical AFM order in certain temperature (T) ranges. We identify the valence bands that form the nesting FS sheets and we point out the differences to the FS of Gd metal lacking FS nesting. We also show that FS nesting is absent in the FM phases of Tb and Dy metal due to magnetic exchange splitting. Hence, the disappearance of FS nesting is identified as the most probable driving force behind the AFM-to-FM phase transitions.

The experiments were performed at beam line 7.0.1 of the Advanced Light Source, Lawrence Berkeley National Laboratory, U.S. The samples studied were single-crystalline 10-nm-thick films, grown *in situ* on a W(110) crystal. Photon energies from 85–135 eV were applied, in combination with a low-T goniometer providing all three angular degrees of freedom; we used angular steps of 0.25°

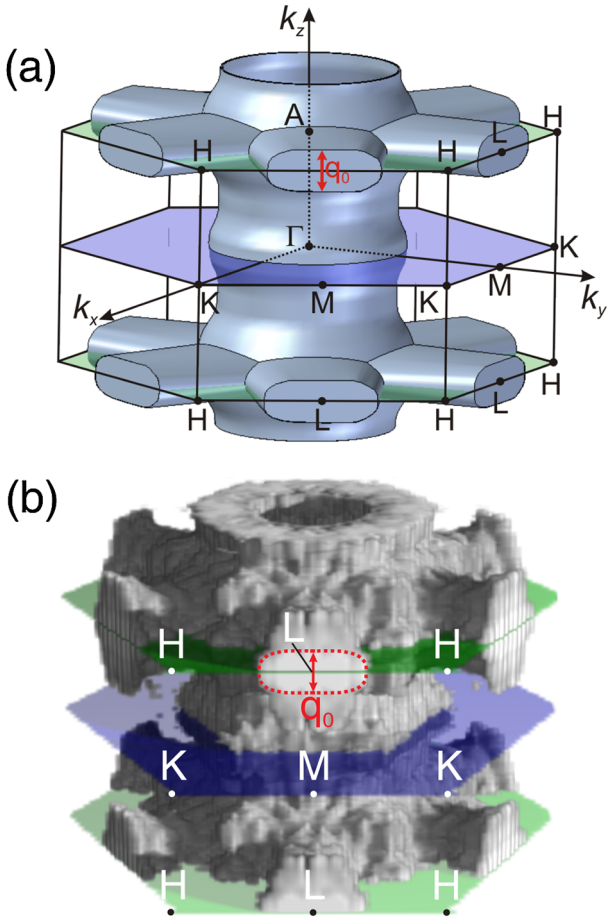

FIG. 1 (color online). (a) Schematics of the FS of Tb metal in the PM phase, derived from the data of this work. The hexagonal BZ boundaries are indicated by solid lines, with the high-symmetry points marked. FS nesting is present around the L point, with the nesting vector $\mathbf{q_0}$, connecting almost parallel sections of the FS. (b) Regions of high PE intensity at $E = E_F$ for Tb metal, reflecting the FS at 240 K in the PM phase; for details, see text. Note that high (low) PE intensity corresponds to light gray (dark gray) tones (i.e., the contrast is opposite of that in Fig. 2).

at a total-system energy resolution of ≅50 meV (full width at half maximum). In this way, a large angular region covering several BZ could be scanned. The surface cleanliness of the samples over data-taking periods up to 15 h between consecutive preparation cycles (base pressure in the UHV chamber: low 10^{-11} mbar) was monitored by photoemission (PE) from electronic states down to 40 eV below the Fermi level (E_F)—via surface states, surface core-level shifts, and PE peaks originating from oxygen or hydrogen adsorption. Despite a slight decline of the surface quality, no significant changes of bulk states relevant to this work were observed. The data were subsequently transformed to $\mathbf{k}$ space to provide direct access to the FS and the Δ_2-like valence bands of the heavy Ln metals [12].

Regions of high PE intensity at $E = E_F$ for Tb metal in the PM phase are displayed in Fig. 1(b). The data cover a complete BZ and reveal the shape of the FS; they are also the basis for the schematics of the FS of Tb metal in the PM state shown in Fig. 1(a). It consists of a pillar-shaped structure centered around the ΓA line. In the region close to the AHL plane, extensions are visible that cross the zone boundary close to L and give rise to FS nesting. The dotted line around L in Fig. 1(b) marks the region with highest PE intensities and follows the nested FS sheet in the MKL zone boundary as a guide to the eyes. In order to obtain the 3D image, symmetrization and normalization of the data was performed. To this end, we picked the irreducible part of the BZ, i.e., the wedge spanned by triangle ΓMK and line ΓA, and—by exploiting the symmetry of the hexagonal lattice—we repeated, i.e., mirrored, the data to cover a complete BZ. For all slices parallel to ΓMK (constant k_z), the PE intensities were normalized to the range from 0 to 1, with 0 being the lowest and 1 the highest measured intensity in the respective slice. This data treatment leads to the required normalized distribution of PE intensities; for further details, see Ref. [9].

Theory predicts that two bands contribute to FS nesting in Ln metals [8]. Because of intrinsic broadening of the Fermi contours perpendicular to the sample surface by $\Delta k_z \cong \pm 0.05$ Å^{-1}, induced by the short escape depth of the photoelectrons [12], PE cannot resolve separate contributions of the two bands (nor does positron annihilation [8]). Additional broadening of the FS features is caused by the residual ΔE_{ex} present in the PM phase [14,15] as well as by phonon broadening at room temperature. The extent of the nested FS sections found for Tb metal is considerably smaller than that of Y metal [7]. Size and shape resemble that found for the $Gd_{0.7}Y_{0.3}$ alloy [8], which is at the onset of helical AFM ordering, in the sense that $Gd_{1-x}Y_x$ alloys with $x > 0.3$ were found to develop a helical AFM phase [16]. This means for Tb that nesting induces a weak driving force for helical AFM ordering, which predominates just in the small T range, from the Curie temperature $T_C = 220$ K to the Néel temperature $T_N = 230$ K [1].

The crucial difference between the FS of Gd and Tb in the PM phase is the absence of FS nesting in Gd due to a different dispersion of the Fermi contours in the region close to the AHL zone boundary. This can be seen clearly in cuts of the FS with the ΓLM plane displayed in Fig. 2 for Gd, Tb, and—for comparison—also for Dy. In the case of Gd ($T_C = 293$ K [1]), Fig. 2(a), the Fermi contour crosses the zone boundary close to the center of the AL line. The Fermi contour of Tb, Fig. 2(b), has a similar shape in the vicinity of the ΓM line, but turns towards the ML zone boundary when the AL line is approached, and it crosses the ML line close to L, causing a nesting of the FS. The PE data for Dy metal ($T_C = 89$ K, $T_N = 179$ K [1]) in Fig. 2(c) reveals that its FS is similar to that of Tb, again with nesting around L. For Tb and Dy, we find z components of the nesting vectors $|\mathbf{q_0}| = 0.2 \pm 0.1$ Å^{-1}. Connecting $\mathbf{q_0}$ with the period of the helix in the AFM

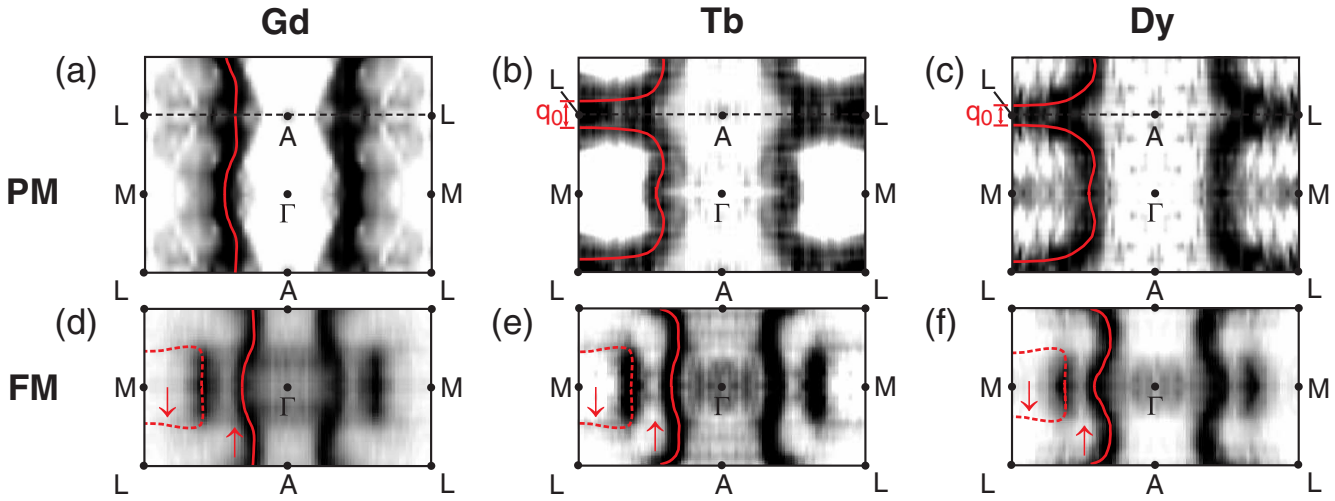

FIG. 2 (color online). Fermi contours in the ΓLM plane of the BZ for (a),(d) Gd metal (see Ref. [9]), (b),(e) Tb metal, and (c),(f) Dy metal in the PM phases (top row), and FM phases (bottom row), respectively; lines serve as a guide to the eyes. The darkness of the gray tones is proportional to the PE intensity. In the PM phase, the contour of (a) Gd ($T = 300$ K) crosses the zone boundary close to the center of the AL line, whereas for (b) Tb ($T = 240$ K) and (c) Dy ($T = 200$ K) it disperses towards L crossing the zone boundary on the ML line, close to L. This behavior in the case of Tb and Dy leads to the formation of nesting sheets of the FS around L, with the nesting vector $\mathbf{q_0}$, indicated by arrows close to L in (b) and (c) (note that for clarity the data were mirrored around the ΓM, ΓA, and AL lines). The exchange-split Fermi contours are shown in the FM phases in the same BZ plane for (d) Gd at 50 K, as well as (e) Tb and (f) Dy metal, both at 25 K. Note the very similar FS of the three metals in the FM phases, with the small differences caused by different ΔE_{ex} and slightly different dispersions.

phase results in turn angles per monolayer of $30 \pm 15°$, which agrees within the error bars with the results of neutron scattering experiments [17,18]. Note that values of $|\mathbf{q_0}|$ determined by ARPES have relatively large error bars due to the large momentum broadening, Δk_z, perpendicular to the sample surface. The advantage of ARPES, however, lies in providing a comprehensive picture of the FS shape. The present observations, i.e., nesting around L for Tb and Dy in the PM phase and absence of nesting for Gd, are in accordance with theory, and identify those parts of the FS that are commonly believed to drive the helical AFM ordering in heavy Ln metals.

Long-range magnetic order in the low-T phase severely alters the shape of the FS. Magnetic exchange splitting, ΔE_{ex}, increases when T is reduced, independent of the type of magnetic ordering (AFM or FM), and ΔE_{ex} follows the same magnetization curve for Gd, Tb, Dy, and Ho if T is scaled to the highest ordering temperature T^* and if it is normalized to $\Delta E_{ex}(T = 0)$ [19]. In the case of Tb and Dy metal, nesting is caused by a band that—if no or only a small ΔE_{ex} is present—is unoccupied on the AL line and crosses E_F on the ML line, close to L [4] [see schematics, Fig. 3(a)]. With increasing ΔE_{ex} at lower temperatures, the majority (↑) subband lowers its energy relative to E_F. At lowest temperatures, it is occupied at L and crosses E_F on the AL line, close to A. The minority (↓) subband behaves oppositely; i.e., its energy increases and the crossing with E_F moves further away from L, towards the M point [see Fig. 3(b)]. This behavior leads to the disappearance of FS nesting at a certain value of ΔE_{ex} and is most probably the main reason for the AFM-to-FM phase transition in heavy Ln metals [4].

Figures 2(d)–2(f) show the effects of magnetic exchange splitting on the Fermi contours of Gd, Tb, and Dy in the ΓLM plane of the BZ. A comparison with the PM phase reveals that nesting around L has vanished for Tb and Dy, as expected from the model discussed above on the basis of Fig. 3, and all three metals have similar FS in their FM phases. The ↑ contour (solid line) is located closer to the ΓA line and crosses the zone boundary closer to A. The ↓ contour (dashed line) disperses in the vicinity of the ΓM line parallel to ΓA, as is visible with high PE intensity. It then turns towards the ML zone boundary with a dispersion parallel to ΓM; in this region it has very low PE intensity,

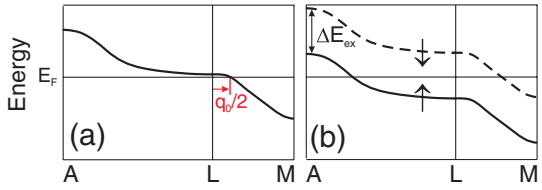

FIG. 3 (color online). Schematics of the influence of magnetic exchange splitting on the valence band that causes FS nesting in Tb and Dy metal. (a) In the PM phase, the band is unoccupied at L and crosses E_F on the ML line at a distance of $|\mathbf{q_0}|/2$ from L. (b) Exchange splitting in the FM phase lowers the energy of the majority subband (solid line) and increases that of the minority subband (dashed line). Hence, the crossings with E_F are shifted against each other, leading to a disappearance of nesting (see text).

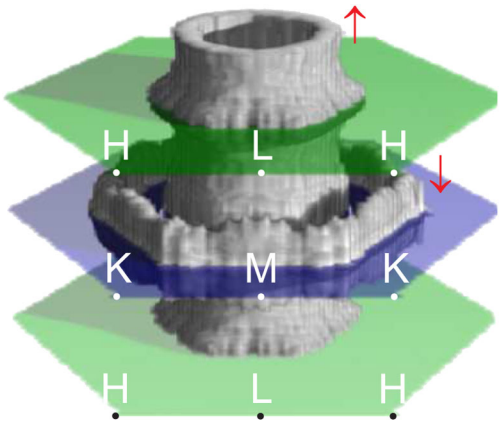

FIG. 4 (color online). Regions of high PE intensity at $E = E_F$ for Tb metal at 25 K, reflecting the FS in the FM phase. Substantial differences to the PM phase [Fig. 1(b)] are obvious, caused by a separation of majority and minority FS sheets by magnetic exchange splitting. In particular, FS nesting around L has disappeared. Note that the sections of the ↓ sheet close to the MLK zone boundary cannot be seen in the 3D plot due to the weak PE signal; its location is visible in the cuts presented in Fig. 2(e). The contrast is the same as that in Fig. 1(b).

only slightly above background, and is visible only for Gd and Tb crossing the zone boundary close to the middle of the ML line (note that the PE intensity in this section is too low to be seen in the 3D plot of Fig. 4). Dy is expected to behave similarly. The exchange splittings of Gd, Tb, and Dy metal at $T = 0$ K, $\Delta E_{\mathrm{ex}} = 0.91$, 0.85, and 0.65 eV, respectively, for the Δ_2 bands at Γ are approximately proportional to the $4f$ spin moments of $7\mu_B$, $6\mu_B$, and $5\mu_B$ per atom [19]. The ↑ and ↓ FS sheets of Dy are therefore closer together than those of Tb and Gd. The tendency to form FS nesting, however, is still present in the ↑ sheets of Tb and Dy, evident by the kinks towards L close to the AL line.

Figure 4 displays the FS of Tb metal in the FM phase. There is clearly no nesting around the L point. The ↑ sheet was pulled back from the L point due to magnetic exchange splitting, forming a pillarlike structure with a smaller diameter than in the PM phase. It is separated from the ↓ sheet that forms a hexagon surrounding the central structure. Note that the shapes of the FS in the FM phases of Tb and Gd [9] are quite similar, with only minor differences.

In summary, we have studied by ARPES the topology of the FS of the heavy Ln metals Gd, Tb, and Dy in both the PM and FM phases. We focused on those valence states that had been identified theoretically as being responsible for the development of a variety of magnetic ordering phenomena in heavy Ln metals. The data for Tb metal cover a complete BZ, providing direct experimental evidence for FS nesting around the L point of the BZ in the PM phase of a pure heavy Ln metal. This confirms the hypothesis that the long-range helical AFM ordering in some of the Ln metals is mainly caused by FS nesting. We also identified experimentally the FS sheet that contributes to nesting, and we showed that its change from the PM to the FM phase is governed by the mechanism discussed first by Liu [4]. It explains how exchange splitting forces nesting to disappear, acting in this way as a driving force behind the AFM-to-FM phase transition. We also pointed out the crucial differences between the FS in the PM phase of Gd on one hand and those of Tb and Dy on the other hand, and we showed that in the FM phase the FS of all three metals are similar. The findings presented here significantly expand the experimental knowledge of FS of heavy Ln metals as well as their role with respect to the variety of magnetic ordering phenomena in heavy Ln metals.

The authors acknowledge the support of S. Kevan, discussions with E. Weschke, G. Bihlmayer, and S. Blügel, as well as the contributions by K. Starke (deceased). Financial support by the Deutsche Forschungsgemeinschaft, Project STA 413/3-1, the German Bundesminister für Bildung und Forschung, Project 05 KS1KEC/2, and the U.S. Department of Energy under Contract No. DEAC03-76SF00098 is gratefully acknowledged.

*Present address: Institut für Experimentelle und Angewandte Physik, Universität Kiel, 24098 Kiel, Germany.

[1] J. Jensen and A. R. Mackintosh, *Rare Earth Magnetism* (Clarendon, Oxford, 1991).
[2] I. D. Hughes *et al.*, Nature (London) **446**, 650 (2007).
[3] A. J. Freeman, in *Magnetic Properties of Rare Earth Metals*, edited by R. J. Elliott (Plenum, London, 1972).
[4] S. H. Liu, in *Handbook of the Physics and Chemistry of Rare Earths*, edited by K. A. Gschneidner, Jr. and L. R. Eyring (North-Holland, Amsterdam, 1978), Vol. 1.
[5] A. V. Andrianov, O. A. Savel'eva, E. Bauer, and C. Paul, Phys. Rev. B **72**, 132408 (2005).
[6] S. B. Dugdale *et al.*, Phys. Rev. Lett. **79**, 941 (1997).
[7] H. M. Fretwell *et al.*, Phys. Rev. Lett. **82**, 3867 (1999).
[8] S. J. Crowe *et al.*, Europhys. Lett. **65**, 235 (2004).
[9] K. M. Döbrich, A. Bostwick, E. Rotenberg, and G. Kaindl, Phys. Rev. B **81**, 012401 (2010).
[10] C. Jackson, Phys. Rev. **178**, 949 (1969).
[11] L. Nordström and A. Mavromaras, Europhys. Lett. **49**, 775 (2000).
[12] K. M. Döbrich *et al.*, Phys. Rev. B **76**, 035123 (2007).
[13] R. Ahuja *et al.*, Phys. Rev. B **50**, 5147 (1994).
[14] E. Weschke and G. Kaindl, J. Phys. Condens. Matter **13**, 11 133 (2001).
[15] K. Maiti *et al.*, Phys. Rev. Lett. **88**, 167205 (2002).
[16] S. Bates *et al.*, Phys. Rev. Lett. **55**, 2968 (1985).
[17] O. W. Dietrich and J. Als-Nielsen, Phys. Rev. **162**, 315 (1967).
[18] M. K. Wilkinson, W. C. Koehler, E. O. Wollan, and J. W. Cable, J. Appl. Phys. **32**, S48 (1961).
[19] C. Schüßler-Langeheine *et al.*, Phys. Rev. Lett. **84**, 5624 (2000).